Journal of GeoEngineering, Vol. 15, No. 2, pp. 89-101, June 2020
http://dx.doi.org/10.6310/jog.202006_15(2).3

DYNAMIC RESPONSE ANALYSIS OF LOESS SLOPE REINFORCED BY FRAME ANCHORS BASED ON NUMERICAL SIMULATION AND SHAKING TABLE TEST

Shuai-Hua Ye [1*], Zhuang-Fu Zhao [2], and Yan-Peng Zhu [3]

ABSTRACT

Loess is a type of porous, weakly cemented sediment. Due to the unique dynamic characteristics of its structure, loess exhibits high seismic vulnerability. Studying the dynamic response of a loess slope supported by frame anchors under earthquake can facilitate the effective seismic design of permanent flexible retaining structures in loess areas. In this paper, the model of a loess slope supported by frame anchors was established by the finite element software PLAXIS 3D, and the results of numerical simulation were verified by a shaking table test. Considering the characteristics of the loess, the dynamic response of the loess slope under earthquake was analysed. The results show that the most dangerous section of the loess slope supported by frame anchors is on the upper part of the slope under the action of earthquake, and the acceleration response of the slope has "amplification effect", "delay effect", and "attenuation effect". The numerical simulation results are in good agreement with the shaking table test results, which can be used as a basis for seismic design of frame anchors in loess areas.

Key words: Loess slope, frame anchors, dynamic response, numerical simulation, shaking table tests.

1. INTRODUCTION

Loess is widely distributed, accounting for 9.8% of the total land area of the Earth. China has the largest loess distribution and thickness in the world. In the loess plateau of northwest China, the construction of civil engineering works inevitably involves a large number of loess-related slopes. Most of the loess areas in China are earthquake-prone areas; historically, there have been many earthquakes, which have caused particularly serious earthquake damage. This severity of damage is closely related to the special structural and dynamic characteristics of loess.

Numerical simulation analyses and shaking table tests are the main means of geotechnical earthquake engineering research. Lin and Wang (2006) studied the dynamic behaviour of the slope through a large-scale shaking table test. Li *et al*. (2017) used shaking table tests to study the dynamic interaction of structure-soil-structure under earthquake excitation. Lin *et al*. (2018) studied the dynamic characteristics of the retaining structure by combining numerical simulation with shaking table tests. Currently, significant research results have been achieved in terms of slope stability, landslide mechanism, slope dynamic response, and slope dynamic characteristics. Biondi *et al*. (2000) studied the seismic response of saturated cohesionless slopes. Lin and Yang (2013) analyzed the dynamic behaviour of railway embankment slope subjected to seismic excitation. Ho (2014) used three-dimensional finite element technology to study the parameters affecting slope stability. Huang *et al*. (2015, 2016) predicted the displacement of slope based on finite displacement method and analysed the stability of geosynthetic-reinforced steep-faced slopes. Based on the response surface approach, Parishad *et al*. (2017) designed the seismic geotechnical robust of cantilever retaining wall. Li *et al*. (2019) studied the dynamic behaviour of soil anchorage landslide at different frequencies. However, the objects of these studies are mostly rock slopes or non-loess slopes.

In the study of loess slopes, as early as 1999, Wang *et al*. (1999, 2001) proposed the mechanism of earthquake-induced high-speed loess landslide, including is loess disintegration, oblique throwing, and dusting effects. Subsequently, researches focused on instability mechanism analysis, damage mechanism analysis, stability analysis, and dynamic response analysis of loess slopes have been continuously developed. Tu *et al*. (2009) analysed the failure mechanism of rainfall-induced landslides. Zhuang *et al*. (2018) studied the distribution and characteristics of loess landslides triggered by the 1920 Haiyuan earthquake. Niu *et al*. (2018) analysed the topographic factors in loess landslide. Qiu *et al*. (2018) studied the response characteristics and preventions for seismic subsidence of loess in Northwest China. However, the effect of retaining structures on loess slopes has not been considered.

In recent years, the popularization and application of flexible retaining structures based on the anchoring technology in slope engineering has brought fresh progress to dynamic analyses of slopes (Han *et al.* 2010; Ye and Zhu 2012; Castorina 2016; Ye *et al.* 2019). As a new type of flexible retaining structures, the frame anchors have played an important role in slope reinforcement engineering in loess areas. Researchers have performed preliminary studies on the seismic response of slopes supported by frames anchors. Zhu and Ye (2011) proposed a simplified analysis method for a slope supported by frame anchors subject to a horizontal earthquake loading. Dong *et al*. (2012, 2013) proposed a simplified seismic

Manuscript received January 23, 2019; revised February 9, 2020; accepted February 27, 2020.
[1*] Professor (corresponding author), School of Civil Engineering, Lanzhou University of Technology, Lanzhou, China (e-mail: yeshuai-hua@163.com).
[2] Graduate student, School of Civil Engineering, Lanzhou University of Technology, Lanzhou, China.
[3] Professor, School of Civil Engineering, Lanzhou University of Technology, Lanzhou, China.

calculation method for the supporting structure of frame anchors. Ye *et al*. (2014) established a dynamic interaction calculation model among fame structure, prestressed anchors and soil under seismic, then, the seismic response of prestress of anchors and the dynamic response of anchors in the anchoring section under simple harmonic earthquake action were solved. However, most of these studies ignore the characteristics of loess, and the research on seismic response still continues to require practical verification.

Based on the finite element analysis software PLAXIS 3D, this paper established a dynamic numerical analysis model of a loess slope supported by frame anchors. Considering the characteristics of loess, the dynamic response laws of a loess slope supported by frame anchors were analysed and verified by shaking table tests. The research results can provide suggestions for the application of the flexible retaining structure of frame anchors in a loess area and evaluate the seismic performance of the anchoring system.

2. CHARACTERISTICS OF LOESS

Loess is a porous, weakly cemented Quaternary sediment, which is characterized by yellowish colour, large pore size, loose structure, vertical joints, containing salts, homogeneous composition without bedding, collapsibility in water, and so on.

2.1 Gravity Erosion in Loess

The complex topography of the loess plateau is caused by long-term severe erosion. In soil erosion, gravity erosion and hydraulic erosion are the two main erosion types, of which gravity erosion has a relatively large proportion, accounting for 28.6% ~ 67% of the total amount of erosion, so the gravity erosion in loess cannot be ignored. Gravity erosion in loess refers to the displacement and destruction of loess due to its own gravity. Gravity erosion on the loess plateau is mainly characterized by loess landslide and collapse (Xu *et al*. 2015).

2.2 Structural Composition of Loess

The structure of the loess is formed by diagenesis after the accumulation of loess. The structure of loess is mainly composed of particles, pores, and aggregates. Most particles are with point-to-point contacts and point-to-surface contacts. The distribution of particles and pores is not uniform. Generally, the pores between the loess particles are large. The loess structure formed in different regions under different geological environments has different characteristics. The structure of loess is closely related to its seismic settlement and collapsible liquefaction. The occurrence of loess collapsibility and soil destruction is essentially the result of the destruction of loess structure (Wang *et al*. 2019).

2.3 Dynamic Characteristics of Loess

The dynamic shear modulus of soil is the dynamic shear stress required to produce the unit dynamic shear strain of the soil, which reflects the ability of soil to resist dynamic shear deformation. The typical curve of dynamic shear modulus of loess with dynamic shear strain is shown in Fig. 1 (Wang *et al*. 2010). It can be seen that the dynamic shear modulus is relatively large under small dynamic shear strain. With the increase of dynamic shear strain, the dynamic shear modulus gradually decreases.

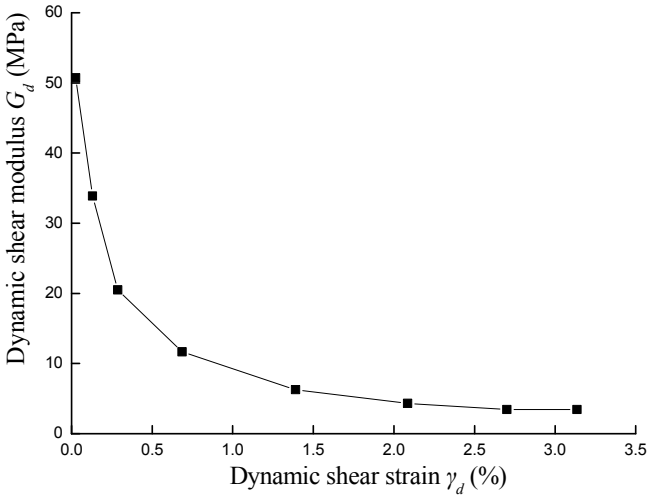

Fig. 1 Typical curve of dynamic shear modulus of loess with dynamic shear strain (Wang *et al.* 2010).

The damping ratio reflects the loss of seismic energy in loess, that is the attenuation degree of seismic wave. Wang *et al*. (2010) obtained the linear relationship between damping ratio and dynamic shear strain of loess through research:

$$\lambda = 0.0344 \log_{10}(\gamma_d) + 0.2912 \tag{1}$$

From Eq. (1), we can see that the damping ratio of loess λ increases with the increase of shear strain γ_d.

3. ESTABLISHMENT OF NUMERICAL MODEL

3.1 Model Size and Cell Division

The finite element analysis software PLAXIS 3D contains many classical and advanced soil constitutive models, which can take into account the interaction between soil and structure and the influence of dynamic loads. It provides a convenient platform for the study of the dynamic response of loess slope supported by frame anchors. According to the research objectives, a three-dimensional model of loess slope supported by frame anchors was established using PLAXIS 3D. The prototype of the model is shown in Fig. 2. In order to keep consistent with the shaking table test model, the model has a slope height of 1.2 metres and an angle of 80 degrees. The anchor has a length of 1.6 m and an angle of 10 degrees in the horizontal direction. The finite element model is shown in Fig. 3. The model is 3.0 m in length, 1.7 m in height, and 1.2 m in width. The mesh size of the model (L_e) is calculated by the following formula:

$$L_e = \frac{r_e}{20} \times \sqrt{(x_{\max} - x_{\min})^2 + (y_{\max} - y_{\min})^2 + (z_{\max} - z_{\min})^2} \tag{2}$$

where ($x_{\max}$, $x_{\min}$, $y_{\max}$, $y_{\min}$, $z_{\max}$, $z_{\min}$) are the boundary dimensions of geometric model; r_e is the relative element size coefficient; r_e = 0.5. The established basic soil element of the grid is a 10-node tetrahedral unit. The soil layer, structural objects, loads, and boundary conditions are automatically considered in the meshing process. The finite element model has a total of 81,502 units and 120,917 nodes.

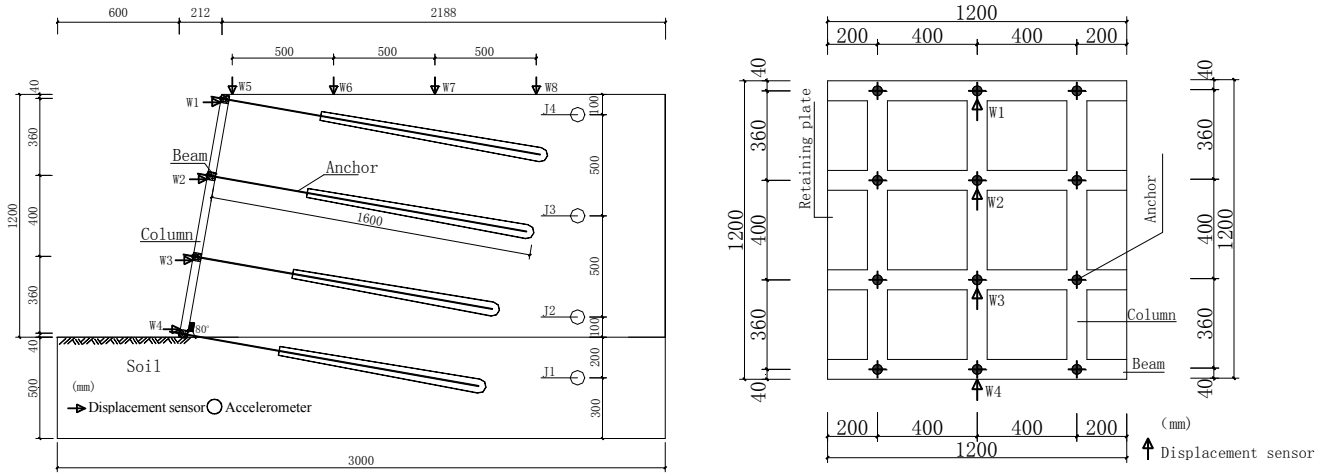

(a) Side view (b) Front view

Fig. 2 Model prototype

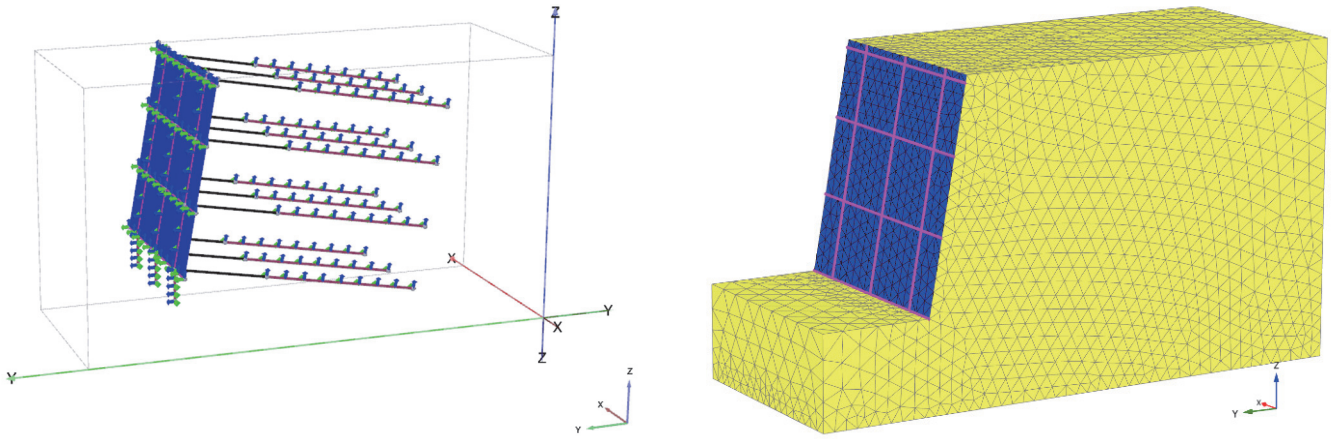

(a) Supporting structure (b) Mesh partition graph

Fig. 3 Finite element numerical model

3.2 Material Parameters and Computational Constitutive Model

Geotechnical materials exhibit obvious non-linear characteristics under loading. These non-linear behaviours can be described by constitutive models. In this paper, loess was used as the soil of the model slope, and the physical and mechanical parameters were obtained according to the shaking table test and the loess geotechnical test.

Mohr-Coulomb strength criterion embodies an elastic-plastic model, in which the shear bearing capacity of soil is taken into account to meet the research needs in calculation and analysis. Therefore, the loess slope model was set up as an elastic-plastic material and Mohr-Coulomb strength criterion were adopted. Considering the initial dynamic characteristics of loess and referring to Wang's research (Wang *et al*. 2010), the dynamic shear modulus of loess is 20 MPa, and the damping ratio is 25%. In the model, the frame comprises beams and columns, which were simulated by the beam element. The retaining plate was simulated by the plate element, the point-to-point anchor element was used to simulate the free section of the anchor, and the embedded beam element was used to simulate the anchoring section of the anchor. The free section and the anchoring section of the anchor were connected through rigid contact. The specific material parameters are shown in Table 2 (Lv *et al.* 2004; Shen and Lv 2010).

3.3 Material Damping

The material damping in dynamic calculation is caused by the viscous properties, friction, and irreversible strain development of soil. The material damping caused by irreversible strain development of soil is not enough to simulate the real soil damping characteristics. Therefore, additional damping is required to simulate the actual damping characteristics. In this paper, this problem is solved by Rayleigh damping. In the analysis of structures and of elastoplastic systems, Rayleigh damping can suppress the system's self-vibration. The Rayleigh damping matrix C consists of a mass matrix M and a stiffness matrix K, *i.e.*, $C = \alpha M + \beta K$, α and β are mass damping constant and stiffness damping constant, respectively. In PLAXIS 3D, the values of α and β can be obtained by inputting the target damping ratio and considering the predominant frequency of the input seismic wave. In this paper, the value of target damping ratio is 25%, and the values of α and β are 1.676 and 0.033, respectively.

Table 1 Soil parameters of the model

Soil name	Unit weight, γ (kN/m^3)	Cohesion, c (kPa)	Internal friction angle, ϕ (°)	Poisson ratio
loess	16.4	18	25	0.35

Table 2 Material parameters of supporting structures

Parameter	Beam, column	Free segment of the anchor	Anchoring section of the anchor	Retaining plate
E (kN/m^2)	2.5×10^7	6.5×10^4	3.0×10^7	1.495×10^6
γ (kN/m^3)	25	–	22	22
Beam type	Predefined	–	Predefined	–
Predefined beam type	Massive rectangular beam	–	Massive circular beam	–
Height (m)	0.8	–	Diameter = 0.15	Thickness = 0.15
Width (m)	0.8	–		
Side friction	–	–	Linear elastic	–
Ultimate side friction of pile top (kN/m)	–	–	200	–
Ultimate side friction of pile bottom (kN/m)	–	–	0	–
Limit reaction force of pile bottom (kN)	–	–	0	–

3.4 Boundary Conditions and Loading Methods

To study the dynamic response of a slope, we must first understand the propagation of seismic waves inside the slope. When using finite element analysis software to simulate and analyse the seismic response of a slope, an artificial boundary should be introduced to make the soil in the calculation area reflect the dynamic response law of the prototype slope as accurately as possible. So, it is necessary to consider the error caused by the reflection or refraction of the seismic wave on the boundary. In dynamic analysis, boundary effects can be reduced by establishing large numerical models. However, it often increases computation time and storage space. Therefore, the viscous boundary and free field boundary are typically used to generate an infinite boundary effect to prevent the distortion or reflection of seismic waves. In this paper, the model used viscous boundary conditions. The model lateral boundary conditions are normally fixed, the bottom boundary is completely fixed, and the top of the model is a free boundary.

In the numerical simulation, the El-Centro wave was input with a peak value of 0.30 g and a duration of 10 s. The curve of acceleration time history and Fourier spectrum are shown in Fig. 4 (we only take the first 10 seconds as seismic excitation). Before the excitation of the seismic wave, the static analysis of the loess slope supported by frame anchors was conducted to study the deformation. Then, based on the static analysis, the local strain was reset, and the displacement was cleared. The dynamic analysis of the slope was performed by inputting the y-direction seismic acceleration at the bottom of the model. The monitoring points were arranged at selected positions on the slope (Fig. 3) to obtain the deformation of the slope after the seismic excitation.

4. SHAKING TABLE TEST

To study the dynamic response of loess slope supported by frame anchors under earthquake conditions, a large-scale shaking table test was performed. The results of the test and numerical simulation are mutually validated to evaluate the seismic performance of the supporting structure. The test was performed on a three-way electro-hydraulic servo-driven seismic simulation shaking table in the Civil Engineering Disaster Prevention and Mitigation Key Laboratory of Lanzhou University of Technology, Gansu Province, China. The test slope is 1.2 m high, and the size of the slope is the same as that of the numerical simulation.

The similarity relations and similarity coefficients of the physical quantities of the model are derived based on the gravity similarity laws and dimensional analysis methods of the landslide model tests (Shen and Lv 2010; Chen *et al*. 2015). Table 3 lists the similitude requirements; among them, elastic modulus E, density ρ, and linear displacement x are controlled by model design. The time t, frequency f, and acceleration a are controlled by dynamic loads. The dimensions of the beams, columns, and plates are converted from that of the actual frame structure according to similarity relations.

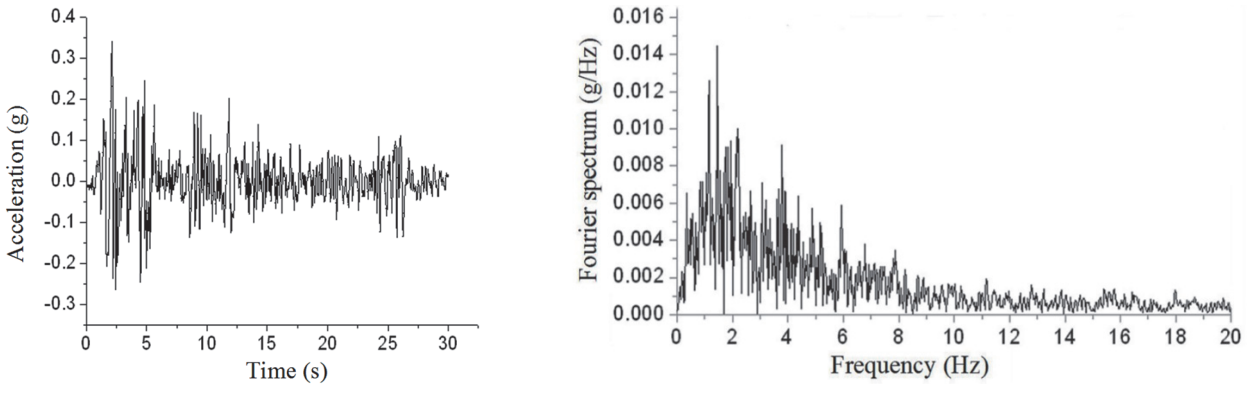

(a) Acceleration time history (b) Fourier spectrum

Fig. 4 Time history of input wave

Table 3 Similarity relationships of the model test

Physical quantities	Similarity relation	Similarity ratio
Strain, ε	$\lambda_\varepsilon = 1.0$	1
Stress, σ	$\lambda_\sigma = \lambda_E$	1/3.612
Elastic modulus, E	λ_E	1/3.612
Poisson ratio, μ	$\lambda_\mu = 1.0$	1
Density, ρ	λ_ρ	1
Length, l	λ_l	1/10
Area, s	$\lambda_S = \lambda_l^2$	1/100
Linear displacement, x	$\lambda_X = \lambda_l$	1/10
Angular displacement, β	$\lambda_\beta = 1.0$	1
Concentrated force, p	$\lambda_P = \lambda_E \lambda_l^2$	1/361.2
Surface load, q	$\lambda_q = \lambda_E$	1/3.612
Mass, m	$\lambda_m = \lambda_\rho \lambda_l^3$	1/1000
Stiffness, k	$\lambda_k = \lambda_E \lambda_l$	1/36.12
Time, t	$\lambda_t = (\lambda_m/\lambda_k)^{1/2}$	0.190
Frequency, f	$\lambda_f = 1/\lambda_t$	5.262
Damping, c	$\lambda_c = \lambda_m/\lambda_t$	0.00526
Velocity, v	$\lambda_v = \lambda_l/\lambda_t$	0.526
Acceleration, a	$\lambda_a = \lambda_l/\lambda_t^2$	2.770

Since the test only considers the horizontal seismic action, in order to minimize the boundary effect and ensure the soil in the model to have the same deformation as the prototype loess slope under the earthquake as much as possible, a 100 mm thick polystyrene foam board was attached to the side walls of the model box along both horizontal vibration directions, so the two side walls become flexible boundaries to reduce the influence of the boundary effect. In addition, the gravel was glued with epoxy resin on the bottom plate surface of the steel plate to make it a rough surface to reduce the relative displacement of the contact surface between the model box and the loess (Xu *et al*. 2008).

Additionally, in order to consider the "remoulding effect" of the soil, the completed model could only be tested after standing for more than 24 hours. The model material was sampled for geotechnical testing, and the physical and mechanical parameters of the model material obtained are shown in Table 1. The model soil is layered into the model box and evenly tampered to ensure that the field compaction rate reaches 90%. The simulated material of anchor is steel wire for prestressed concrete with diameter of 5 mm, and its tensile strength is not less than 1570 kPa. The arrangement of measuring points is the same as that in numerical simulation. The shaking table model is shown in Fig. 5.

In the shaking table test, the El-Centro wave, Lanzhou wave and Wenchuan wave were selected as seismic excitations. The test was loaded with different spectral characteristics, ground motion intensity, and duration of input seismic waves. In the course of the experiment, when the acceleration peak or the type of seismic wave changed, a slight white noise excitation was added to eliminate the residual effects of seismic excitation and reduce the test error. To facilitate comparison with the numerical simulation, only the El-Centro wave with an input acceleration peak of 0.15 g was adopted as the seismic wave for analysis. The research result of the shaking table test on the loess slope supported by frame anchors will be presented in another paper.

(a) Anchors (b) Frame (c) Treatment of bottom boundary

(d) Treatment of side boundary (e) Completed model

Fig. 5 Shaking table test

5 COMPARISON OF NUMERICAL SIMULATION AND EXPERIMENTAL RESULTS

Through numerical simulation, firstly, the static stability of the slope under self-weight was studied. Then, seismic excitation was input to analyse and compare the deformation characteristics under static and dynamic loads. In addition, the dynamic response of the loess slope supported by the frame anchors was analysed. Finally, the shaking table test was used to verify the results.

5.1 Static Calculation Results

According to the numerical simulation results, the contour of horizontal displacement and vertical displacement of the slope could be obtained (Fig. 6). It can be seen that the displacement of the slope under static force is very small, and the horizontal displacement of the slope under static action is primarily concentrated at the toe of the slope, with a maximum of 0.30 mm. The top of the slope has micro-sedimentation, and the bottom of the slope is slightly uplifted. The vertical displacement is concentrated in the lower part of the slope, and the maximum displacement at the toe of the slope is 0.18 mm. In addition, the distribution of vertical displacement presents an arc-shaped block area, with the displacement gradually decreasing from the surface of the slope to the interior of the slope body.

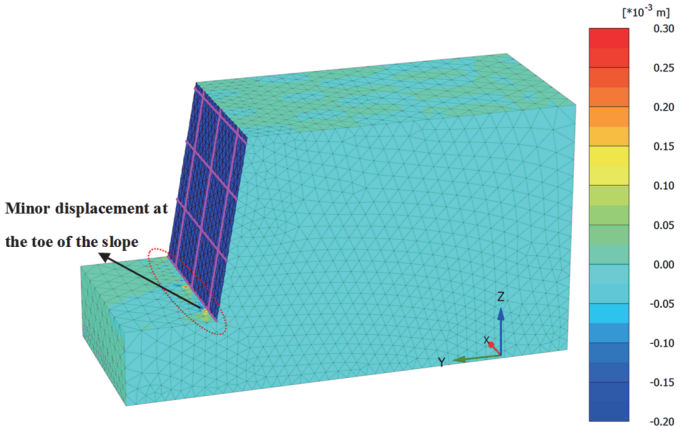

(a) Horizontal displacement contour

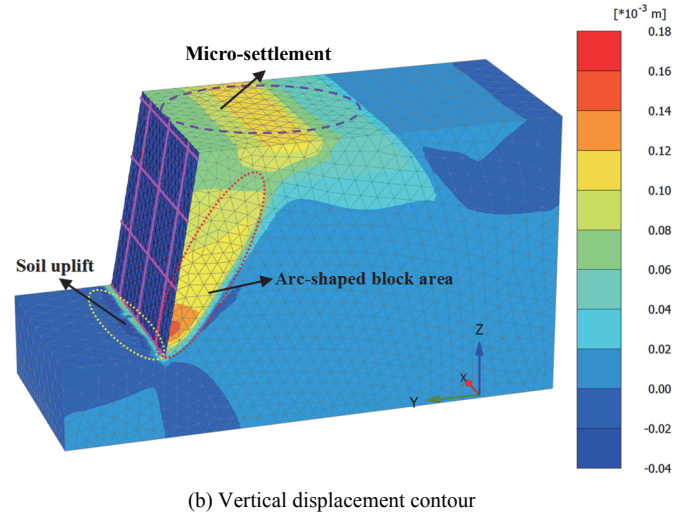

(b) Vertical displacement contour

Fig. 6 Displacement contour under static excitation

Loess mostly has loose soil and low strength (refer to Section 2.1). Under the action of self-weight, the soil is gradually compacted. At the same time, the force is transmitted downward and to the free surface of the slope, and the force is concentrated at the toe of the slope. The soil behind the supporting structure applies pressure to the empty surface of the slope and to the toe of the slope due to the gravity erosion in loess (Fig. 7), which is finally reflected in the form of slight uplift at the toe of the slope. Under the action of static force, the displacement value is small, and the slope remains generally stable.

5.2 Dynamic Calculation Results

Displacement Response of Slope

The mesh deforming graph of the slope after the earthquake is shown in Fig. 8. Comparing with the grid map before the earthquake, it can be found that the top of the slope has settlement, and the toe of the slope protrudes towards the free surface.

The displacement contour of the slope and the corresponding displacement curves under earthquake are shown in Figs. 9 and 12. As shown in Fig. 9(a), the maximum horizontal displacement of the slope occurs near the top of the slope after the action of the seismic waves. However, under the action of static force, the maximum horizontal displacement occurs at the toe of the slope (as shown in Fig. 6(a)). That is to say, the most dangerous section of the loess slope system strengthened by the frame anchors moves up under the action of earthquake, and the most dangerous position is in the upper part of the slope. From Fig. 9(b), the maximum horizontal displacement reaches 19.82 mm at the measuring point *W*1, while the displacement of the lower part of the slope is very small, even negative.

The negative horizontal displacement indicates that the soil moves along the Y axis, that is towards the inside of the slope. It indicates that the supporting structure of the frame anchors plays a significant role under the earthquake. Under the action of dynamic load, the slope body generates relative displacement and moves outward. At the same time, the active earth pressure acts on the supporting structure, and the anchor enters the working state. The force is transmitted to the anchor and then gradually transmitted to the stable soil layer along the length of the anchoring section. Finally, the frame and the slope move towards the inside of the slope, and the displacement has a negative value (Fig. 10).

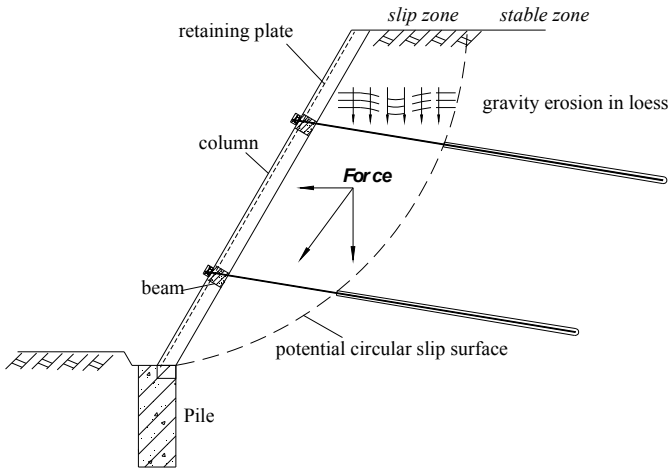

Fig. 7 Propagation mechanism of force under static excitation

The horizontal displacement near the slope surface is smaller than the area inside the slope surface, and an area of arc-shaped belt is formed inside the slope body (Fig. 9(a)). Figure 11 shows the shear strain increment of the slope, it can also be noted that the shear strain increment forms an obvious arc-shaped belt region inside the slope body and passes through the toe of the slope. The deformation in this area is more significant than in other areas, while the deformation of soil outside the area is relatively small. This indicates that the area near the slope surface remains in the elastic deformation zone, while the arc-shaped belt area is in the plastic zone, *i.e.,* the potential slip zone of the slope.

Figure 12(a) shows the contour of the vertical displacement at the top of the slope under earthquake. Combining with Fig. 12(b), it can be noted that the vertical displacement of the top of the slope fluctuates with time. The farther away from the slope shoulder, the smaller the vertical displacement, and the maximum vertical displacement at the top of the slope is 11.36 mm.

The vertical displacement inside the slope gradually decreases as it moves away from the slope surface. Its maximum vertical displacement reaches 12.00 mm, which occurs in the middle and lower part of the slope (Fig. 12(a)). It reflects the phenomenon of stress concentration at the toe of the slope under the action of self-weight and earthquake. Unlike the arc-shaped massive plastic region under static action, the plastic region under seismic action is layered in an arc-shaped belt region.

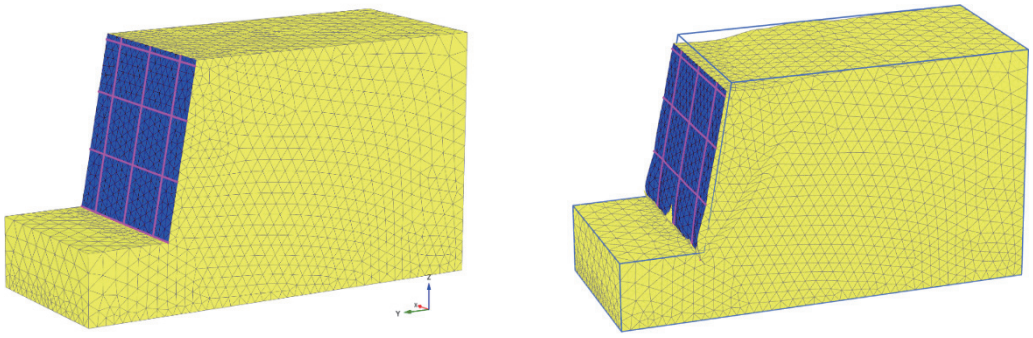

(a) Before the earthquake (b) After the earthquake

Fig. 8 Mesh deforming graph

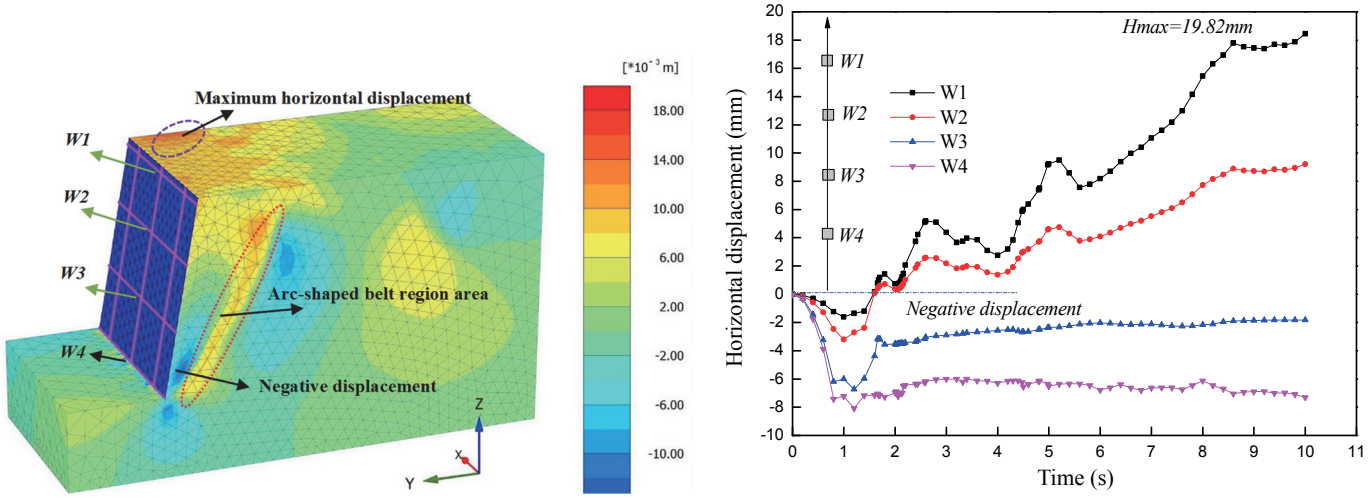

(a) Horizontal displacement contour (b) Horizontal displacement history

Fig. 9 Horizontal displacement

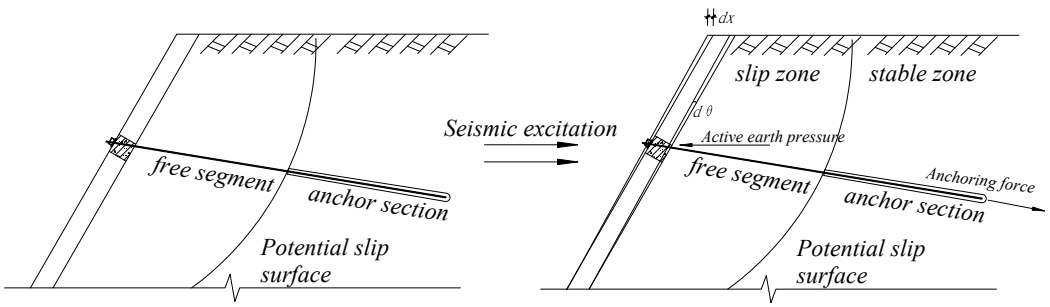

Fig. 10 Propagation mechanism of force under seismic excitation

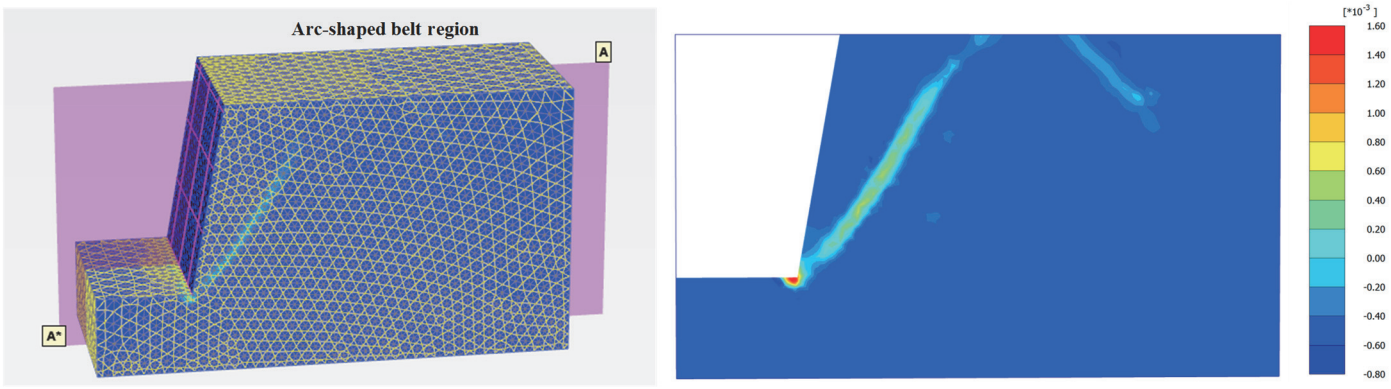

(a) Shear strain increment (b) Profile A-A

Fig. 11 Shear strain increment

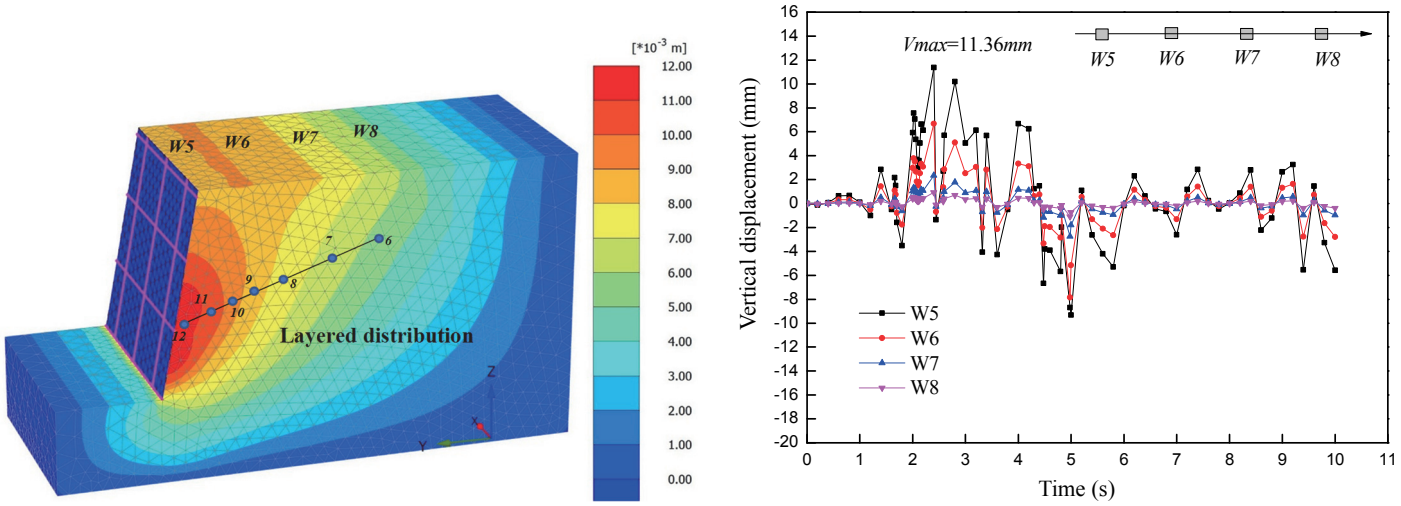

(a) Vertical displacement contour (b) Vertical displacement history

Fig. 12 Vertical displacement

Response of Acceleration

The acceleration response of slope related to the seismic inertial force is the basic index for evaluating the seismic dynamic response of the slope. The acceleration time history curve obtained by numerical simulation is shown in Fig. 13. As shown in the figure, from the bottom to the top of the slope, the peak acceleration increases continuously. The peak acceleration of J1 at the bottom of the slope reach 0.205 g, and the peak acceleration of J4 at the top of the slope reach 0.419 g. It indicates that the "amplification effect" of the slope is obvious under the action of seismic waves.

In addition, the acceleration response has a "delay effect". The time of peak acceleration of J1, J2, J3, and J4 are 0.3 s, 0.5 s, 0.8 s, and 1.3 s, respectively. It can be seen that the time interval between acceleration peaks is increasing. This can be attributed to the internal damping of the loess and the transit time difference of seismic waves. The "delay effect" of acceleration indicates that the slope is vibrating asynchronously at different heights; therefore, in actual engineering, the integrity of the supporting structure needs to be strengthened to reduce the slope failure caused by the asynchronous vibration of the slope due to the "delay effect".

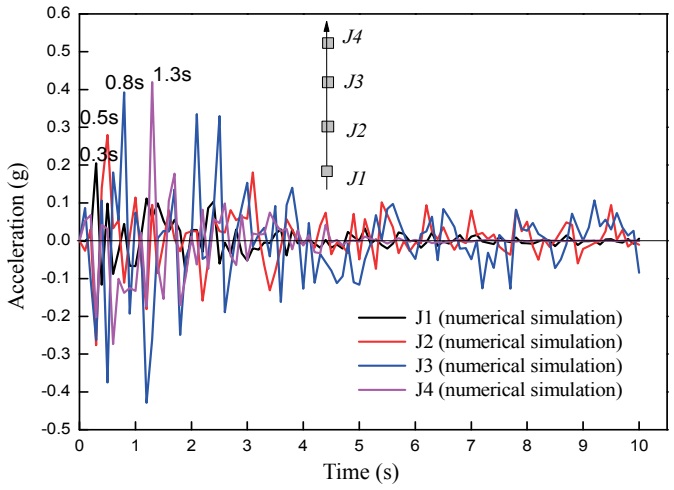

Fig. 13 Acceleration history of numerical simulation

In order to compare with numerical simulations, the acceleration time history curves of points J2 and J4 in the shaking table test are provided. The duration of the shaking table test is 60 s, and the acceleration time history curves obtained are shown in Fig. 14.

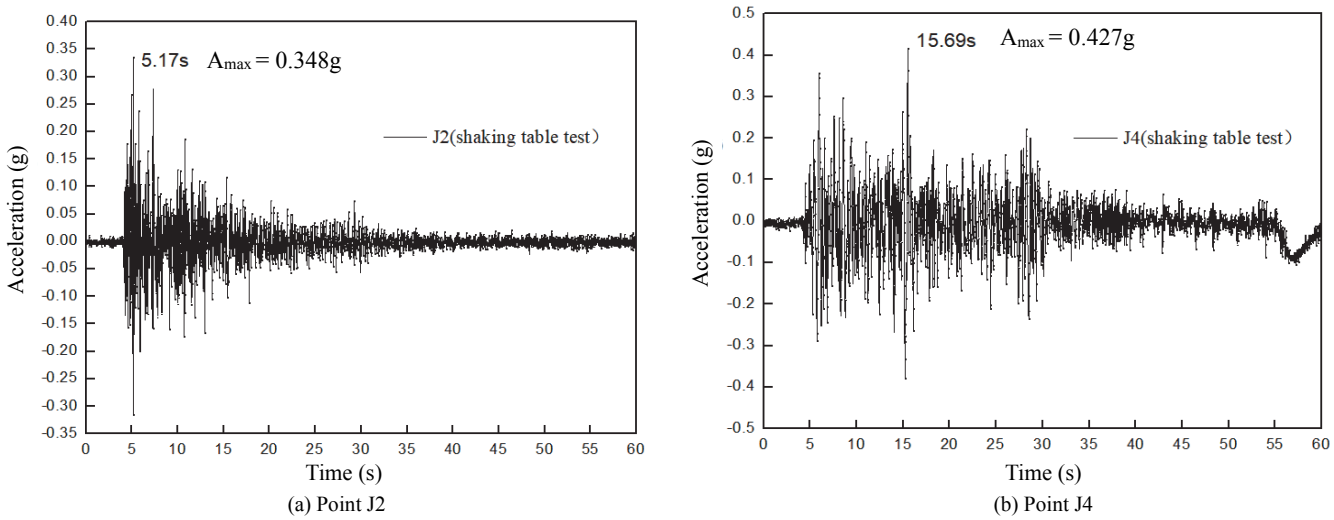

(a) Point J2 (b) Point J4

Fig. 14 Acceleration history of shaking table test

It can be noted that the peak value of the acceleration at point J4 is 0.427 g, and the time of peak acceleration is 15.69 s. The peak value of acceleration at point J2 is 0.348 g, and the peak acceleration appears at 5.17 s, which indicates that the higher the monitoring point, the larger the peak value of acceleration. Additionally, there is a difference in the time when the peak value appears, which is consistent with the change rule of numerical simulation results.

To describe the law of slope acceleration response under seismic action more accurately, the peak ground acceleration amplification coefficient (M_{PGA}) was defined as the ratio of the acceleration peak value of the measured dynamic response at each monitoring point P_{Ai} to the input acceleration peak value P_{A0}.

$$M_{PGA} = P_{Ai} / P_{A0} \tag{3}$$

The M_{PGA} measured by numerical simulation and shaking table test is shown in Fig. 15. As shown in the figure, the numerical simulation results are similar to shaking table tests. When h/H is 0.5, the M_{PGA} is smaller than the value for h/H = 1.0 (where h is the position of the measuring point, and H is the total height of the model). In the range of slope height, the M_{PGA} exhibits a drum-like distribution. The amplification factor at the lower part of the slope is less than 1.0, and PGA "attenuation effect" exists.

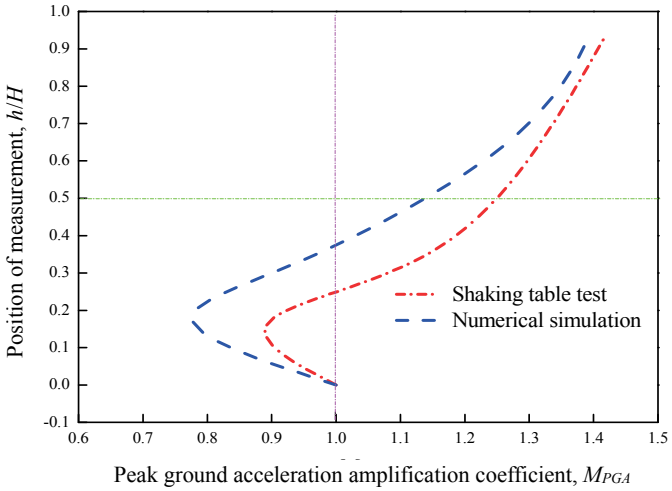

Fig. 15 Peak ground acceleration amplification coefficient

The amplification effect of PGA depends on the proximity of the natural frequency of slope and the main frequency of load. The closer the two, the more obvious the amplification effect. On the contrary, when the amplification effect is weak, the case of response attenuation and amplification coefficient less than 1.0 will occur (Wang *et al*. 2018).

It can also be observed in Fig. 15 that the M_{PGA} of the numerical simulation is smaller than the results of the shaking table test. In the numerical simulation, the soil parameters do not change during the earthquake. However, in the shaking table test, the parameters of the soil actually changed due to the earthquake; therefore, the acceleration response is different from the numerical simulation.

Stress Analysis of Frame Columns

The slope maintains a stable state under natural conditions and has a certain degree of anti-sliding force. After the supporting structure is applied, the slope will generate more sliding force because of the deterioration of the surrounding environment and other conditions. As a force transmission structure in the supporting structure of frame anchors, the frame distributes the excess sliding force or earth pressure of the slope body to the adjacent anchors, then it transmits the force by the anchors to the stable soil through the gripping force between the anchoring section and the mortar as well as the friction force between the anchors and the surrounding soil body. Thus, the slope is in a stable state under the anchoring effect.

Previous studies have shown that the frame beam is an auxiliary force-bearing member that only plays a spatial synergistic role (Dong *et al*. 2014). Therefore, only the frame column is investigated here. Figure 16 shows the envelope diagram of the shear force and the bending moment of the column according to the numerical simulation. The shear value Q_{max} is 69.9 kN, the Q_{min} is – 108.9 kN, the bending moment value M_{max} is 179.5 kN·m, and the M_{min} is – 24.34 kN·m. As can be noted in the Fig. 16, the positive and negative shear forces are alternately distributed along the height of the column, and a sudden change occurs near the position of anchors.

Figure 17 shows the strain distribution along the height direction of the column in the shaking table test. It can be noted that the strain distribution is alternatively distributed in positive and negative

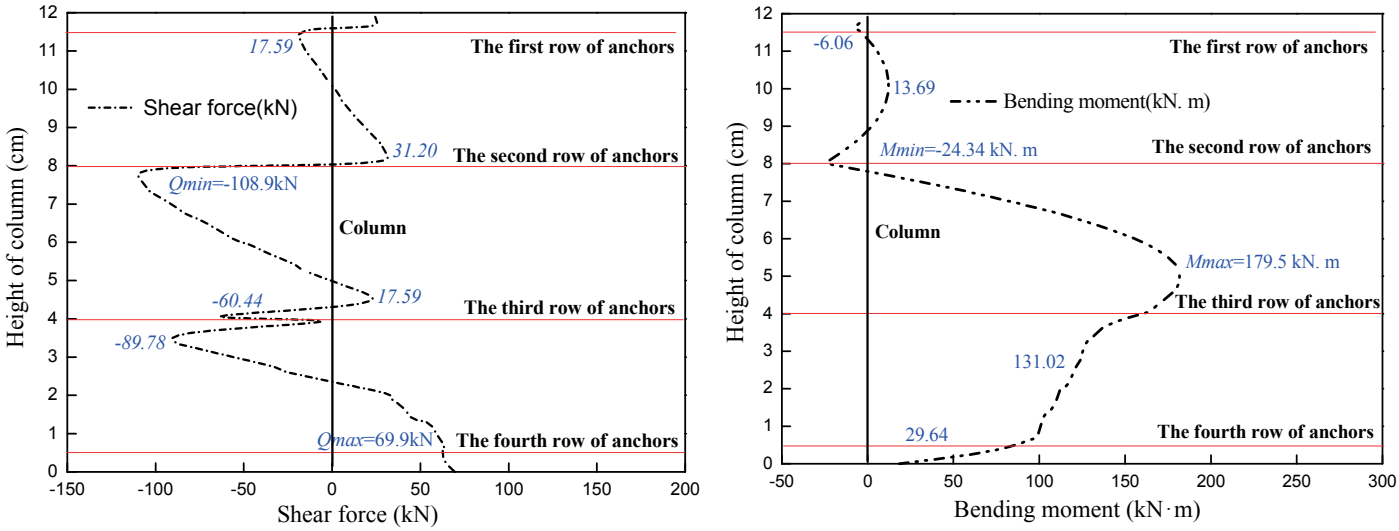

(a) Envelope diagram of shear force

(b) Envelope diagram of bending moment

Fig. 16 Distribution of bending moment and shear force of columns

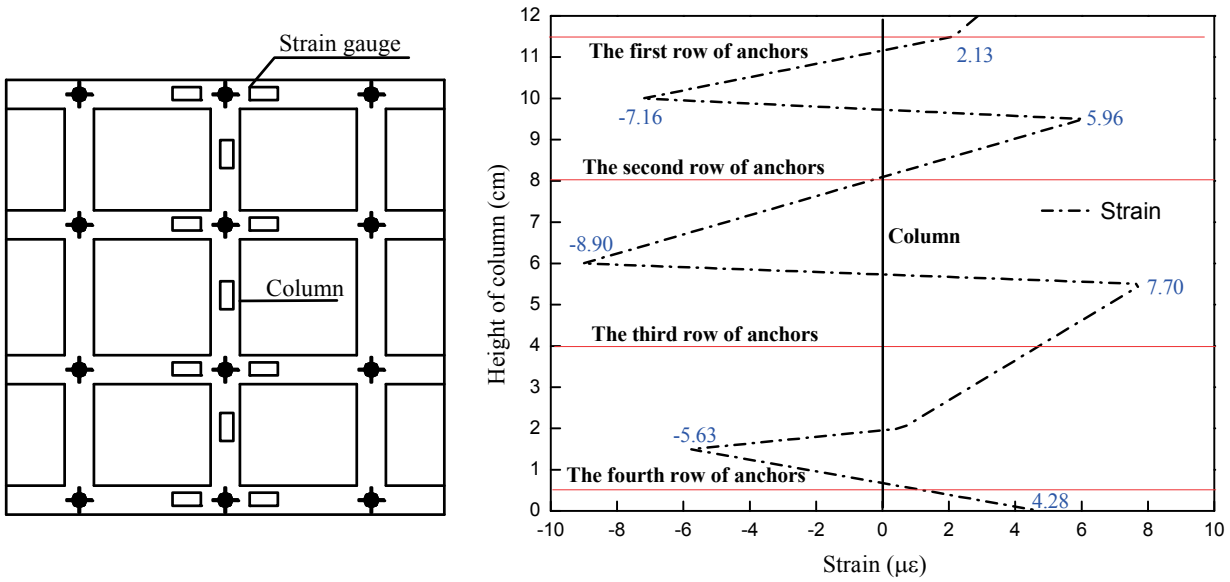

(a) Strain monitoring points (shaking table test)

(b) Strain distribution of the column

Fig. 17 Strain distribution of the column (shaking table test)

directions, which is similar to the distribution of shear force in the numerical simulation. From the distribution of numerical values (Figs. 16 and 17), the values at both ends of the column are smaller than those in the middle. That is, the shear force, bending moment, and strain of the column all correspond to the form of "small in both sides and large in the middle".

Analysis of Internal Force of the Anchor

The internal force of the anchor obtained by numerical simulation is provided in Fig. 18. It is found that the axial force, shear force, and bending moment of the anchor are enlarged to different degrees under the excitation of seismic waves.

Since the free section of the anchor and the anchoring section of the anchor are simulated by different elements in the software of PLAXIS 3D, the free section of the anchor is equivalent to a linear spring, and its axial force does not change. Therefore, this paper provides a numerical simulation of the distribution of the axial force of the anchorage section (Fig. 19). It can be observed that the maximum axial force of the anchor appears at the junction of the free section and the anchoring section.

From the numerical distribution in Fig. 18(a), after the earthquake, the axial forces of the anchors in rows 1, 2, 3, and 4 were 135.6, 206.1, 299.7, and 225.5 kN, respectively. The numerical distribution of axial force of the anchor from top to bottom along the slope height exhibits a feature of "smaller-larger-larger-smaller" variation, and the maximum axial force appears in the third row of anchors. Figure 19 shows the axial force distribution of the anchor in the middle of the frame of the shaking table test model. The relationship between the axial force and strain of the anchor can be reflected by the following formula:

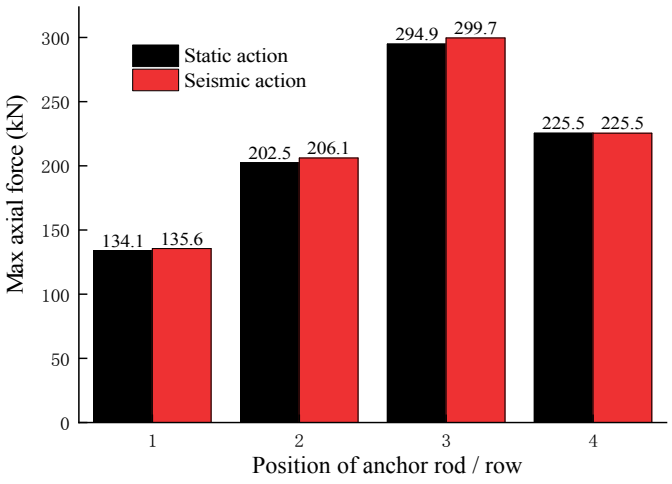

(a) Axial force

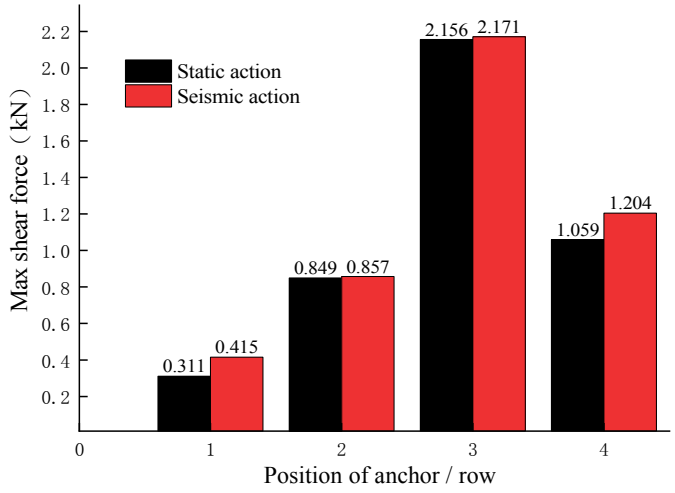

(b) Shear force

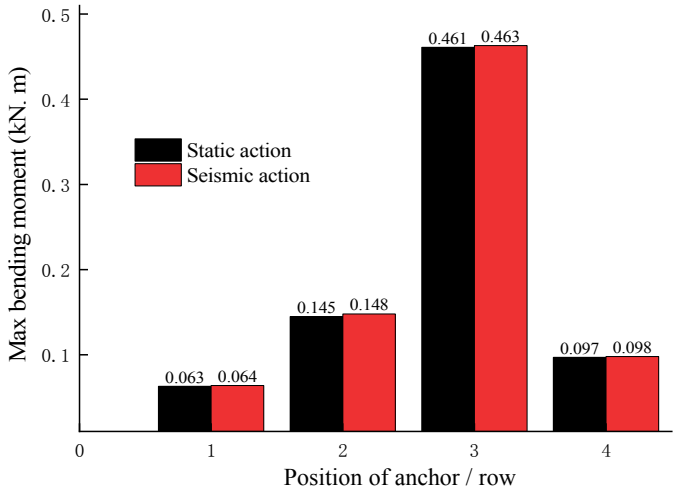

(c) Bending moment

Fig. 18 The internal force of the anchor

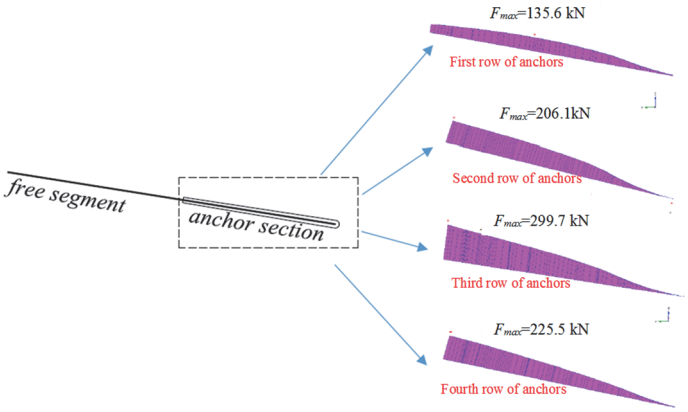

Fig. 19 Axial force distribution of anchors (numerical simulation)

$$F = E_a \varepsilon A_r \tag{4}$$

where F is the axial force of the anchor; E_a is the elastic modulus of anchor; ε is the strain of the anchor; A_r is the sectional area of the anchor. As can be seen from Eq. (4), the strain of anchor can reflect its axial force response. It can be noted that the maximum strain also appears in the third row. Adopting one of the rows of anchors (such as the third row) as the research object, it can be observed that the strain distribution along the long direction of the anchor presents a "single peak" variation, and the strain peak appears at the junction of the free section, and the anchoring section and its maximum strain is 230.75 με.

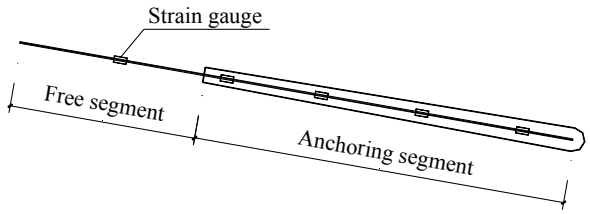

(a) Strain monitoring points (shaking table test)

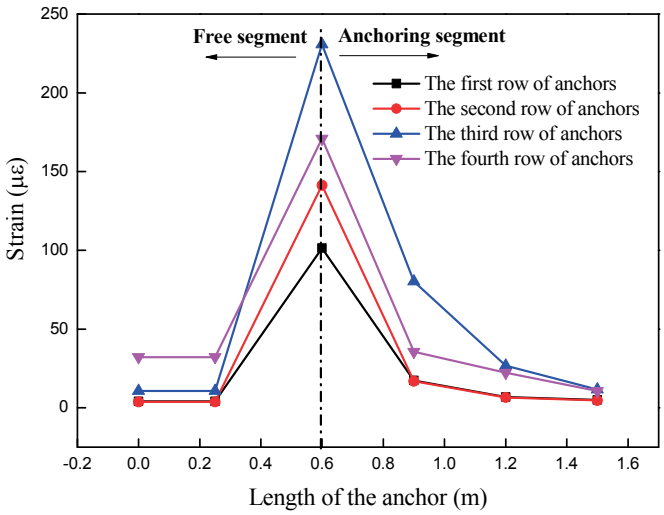

(b) Strain distribution of anchors

Fig. 20 Strain distribution of anchors (shaking table test)

6. CONCLUSIONS

Through the mutual verification of the numerical simulation and the shaking table test, and considering the characteristics of loess, the dynamic response law of a loess slope supported by frame anchors was analysed. The following conclusions were obtained:

1. The supporting structure of the frame anchors plays a significant role under the earthquake. The most dangerous section of the loess slope system strengthened by the frame anchors moves up under the action of earthquake, and the most dangerous position is in the upper part of the slope. Therefore, the upper part of the slope must be primarily supported.
2. Under the action of earthquake, the loess slope supported by frame anchors has an elastic zone near the slope surface and an arc-shaped belt-shaped plastic zone inside the slope body. The shear strain increment forms an obvious arc-shaped belt region inside the slope body and passes through the toe of the slope, which is a potential slip zone of the slope.
3. Under the action of seismic wave, the "amplification effect" of slope is obvious. In addition, the acceleration response also has "delay effect" and "attenuation effect". In actual engineering, in consideration of "amplification effect", the upper structure of the slope should be strengthened. In addition, the integrity of the supporting structure needs to be strengthened to reduce the slope failure caused by the asynchronous vibration of the slope due to the "delay effect".
4. As the force transmission structure in the supporting structure of the frame anchors, the internal force distribution of the frame column displays the form of "small on both sides and large in the middle" under the earthquake.
5. The distribution of the axial force of the anchor from top to bottom along the slope height exhibits a "smaller-larger-larger-smaller" variation. The strain distribution along the long direction of the anchor presents a "single peak" variation, and the strain peak appears at the junction of the free section and the anchoring section.

FUNDING

The corresponding author is grateful to the National Natural Science Foundation of China (No. 51768040).

ACKNOWLEDGEMENTS

The authors acknowledge the helpful comments on this paper from anonymous reviewers.

DATA AVAILABILITY

All data and/or computer codes used/generated in this study are included in this paper.

REFERENCES

Biondi, G., Cascone, E., Maugeri, M., and Motta, E. (2000). "Seismic response of saturated cohesionless slopes." *Soil Dynamics and Earthquake Engineering*, **20**(1-4), 209-215. https://doi.org/10.1016/S0267-7261(00)00051-8

Chen, G.X., Chen, S., Zuo, X., Du, X.L., Qi, C.Z., and Wang, Z.H. (2015). "Shaking-table tests and numerical simulations on a subway structure in soft soil." *Soil Dynamics and Earthquake Engineering*, **76**, 13-28. https://doi.org/10.1016/j.soildyn.2014.12.012

Castorina, S.V. (2016). "An approach to estimate required geosynthetics strength in reinforced slopes with inclined backslope for static and seismic loading." *Journal of Geoengineering*, TGS, **11**(1), 13-25. http://dx.doi.org/10.6310/jog.2016.11(1).2

Dong, J.H., Zhu, Y.P., and Ma, W. (2012). "Simplified seismic design method of frame supporting structure with prestressed anchors for slope stability." *China Journal of Highway and Transport*, **25**(5), 38-46. http://ir.casnw.net/handle/362004/20649

Dong, J.H., Zhu, Y.P., and Ma, W. (2013). "Study on dynamic calculation method for frame supporting structure with prestress anchors." *Engineering Mechanics*, **30**(5), 250-264. http://dx.doi.org/10.6052/j.issn.1000-4750.2012.10.0810

Dong, J.H., Zhu, Y.P., and Ma, W. (2014). "Dynamic caculation method of frame prestressed anchors for slope stability under seismic effect." *Chinese Journal of Rock Mechanics and Engineering*, **33**(S1), 3135-3143. http://dx.doi.org/10.6052/j.issn.1000-4750.2012.10.0810

Han, A.M., Li, J.G., Xiao, J.H., and Xu, H.Z. (2010). "Mechanical behaviours of frame beam supporting structure with prestressed anchors." *Rock and Soil Mechanics*, **31**(9), 2984-2900. http://doi.org/10.16285/j.rsm.2010.09.033

Ho, I-H. (2014). "Parametric studies of slope stability analyses using three-dimensional finite element technique: geometric effect." *Journal of Geoengineering*, TGS, **9**(1), 33-43. http://doi.org/10.6310/jog.2014.9(1).4

Huang, C.-C., and Yeh, S-W. (2015). "Predicting periodic rainfall-induced slope displacements using force-equilibrium-based finite displacement method." *Journal of GeoEngineering*, TGS, **10**(3), 83-89. http://doi.org/10.6310/jog.2015.10(3).2

Huang, C.-C., Huang, B.-S., and Chen, Y.-W. (2016). "Stability analyses for geosynthetic-reinforced steep-faced slopes subjected to toe scouring." *Journal of GeoEngineering*, TGS, **11**(3), 123-132. http://doi.org/10.6310/jog.2016.11(3).2

Lin, M.L. and Wang, K.L. (2006). "Seismic slope behaviour in a large-scale shaking table model test." *Engineering Geology*, **86**(2-3), 118-133. http://dx.doi.org/10.1016/j.enggeo.2006.02.011

Lin, Y.L. and Yang, G.L. (2013). "Dynamic behaviour of railway embankment slope subjected to seismic excitation." *Natural Hazards*, **69**(1), 219-235. http://dx.doi.org/10.1007/s11069-013-0701-3

Li, P.Z., Liu, S.T., Lu, Z., and Yang, J.P. (2017). "Numerical analysis of a shaking table test on dynamic structure-soil-structure interaction under earthquake excitations." *Structural Design of Tall and Special Buildings*, **26**(15). http://doi.org/10.1002/tal.1382

Lin, Y.L., Cheng, X.M., and Yang, G.L. (2018). "Shaking table test and numerical simulation on a combined retaining structure response to earthquake loading." *Soil Dynamics and Earthquake Engineering*, **108**, 29-45. https://doi.org/10.1016/j.soildyn.2018.02.008

Li, N., Wang, B.Q., Men, Y.M., Liu, N.N., Liu, X.L., and Gao, O. (2019). "Dynamic behavior of soil anchorage landslide at different frequencies" *Geomatics Natural Hazards and Risk*, **10**(1), 271-286. http://dx.doi.org/10.1080/19475705.2018.1521878

Lv, X.L., Zou, Y., Lu, W.S., and Zhao, B. (2004). "Experimental study on Shanghai World Financial Center." *Earthquake Engineering and Engineering Vibration*, **24**(3), 57-63. http://doi.org/10.13197/j.eeev.2004.03.008

Niu, Q.F., Dang, X.H., Li, Y.F., Zhang, Y.X., Lu, X.L., and Gao, W.Y. (2018). "Suitability analysis for topographic factors in loess landslide research: A case study of Gangu County, China." *Environmental Earth Sciences*, **77**(7), 294. http://doi.org/10.1007/s12665-018-7462-y.

Parishad, R., Nadarajah, R., and Juang, C.H. (2017). "Seismic geotechnical robust design of cantilever retaining wall using response surface approach." *Journal of GeoEngineering*, TGS, **12**(4), 147-155. http://dx.doi.org/10.6310/jog.2017.12(4).2.

Qiu, J., Wang, X., Lai, J., Zhang, Q., and Wang, J. (2018). "Response characteristics and preventions for seismic subsidence of loess in Northwest China." *Natural Hazards*, **92**(3), 1909-1935. http://dx.doi.org/10.1007/s11069-018-3272-5

Shen, D.J. and Lv, X.L. (2010). "Experimental study on the mechanical property of microconcrete in model test." *China Civil Engineering Jounal*, **43**(10), 14-21. http://dx.doi.org/10.15951/j.tmgcxb.2010.10.013

Tu, X.B., Kwong, A.K.L., Dai, F.C., Tham, L.G., and Min, H. (2009). "Field monitoring of rainfall infiltration in a loess slope and analysis of failure mechanism of rainfall-induced landslides." *Engineering Geology*, **105**(1-2), 134-150. http://dx.doi.org/10.1016/j.enggeo.2008.11.011

Wang, J.D. and Zhang, Z.Y. (1999). "A study of the mechanism of high speed loess landslide induced by earthquake." *Chinese Journal of Geotechnical Engineering*, **21**(6), 670-674.

Wang, J.D., Bai, M.X., and Xiao, S.F. (2001). "A study on compound mechanism of earthquake-related sliding displacements on gently inclined loess slope." *Chinese Journal of Geotechnical Engineering*, **23**(4), 445-449. http://dx.doi.org/10.3321/j.issn:1000-4548.2001.04.013

Wang, J.D., Li, P., Gu, Q., Xu, Y.J., and Gu, T.F. (2019). "Changes in tensile strength and microstructure of loess due to vibration." *Journal of Asian Earth Sciences*, **169**, 298-307. https://doi.org/10.1016/j.jseaes.2018.10.011

Wang, Z.J., Luo, Y.S., Wang, R.R., Yang, L.G., and Tan, D.Y. (2010). "Experimental study on dynamic shear modulus and damping ratio of undisturbed loess in different regions." *Chinese Journal of Geotechnical Engineering*, **32**(9), 1464-1469.

Wang, L.M., Pu, X.W., Wu, Z.J., Xu, S.H., and Liu, K. (2018). "Shaking table tests of dynamic response of loess slopes under the coupling effects of earthquakes and rainfalls." *Chinese Journal of Geotechnical Engineering*, **40**(7), 1287-1293. https://doi.org/10.11779/CJGE201807015

Xu, X.Z., Liu, Z.Y., Xiao, P.Q., Guo, W.Z., Zhang, H.W., Zhao, C., and Yan, Q. (2015). "Gravity erosion on the steep loess slope: behaviour, trigger and sensitivity." *CATENA*, **135**, 231-239. https://doi.org/10.1016/j.catena.2015.08.005.

Xu, G., Yao, L., Gao, Z., and Li, Z. (2008). "Large-scale shaking table model test study on dynamic characteristics and dynamic responses of slope." *Chinese Journal of Rock Mechanics and Engineering*, **27**(3), 624-632. http://dx.doi.org/10.3321/j.issn:1000-6915.2008.03.025

Ye, S.H. and Zhu, Y.P. (2012). "Stability analysis of slope supported by frame with pre-stressed anchors under earthquake." *Journal of China Coal Society*, **37**(12), 1994-1998. http://dx.doi.org/10.1007/s11783-011-0280-z

Ye, S.H., Zhu, Y.P., and Wang, D.Q. (2014). "Seismic interaction analysis model and seismic response analysis of frame-prestressed anchor-soil system." *China Civil Engineering Journal*, **47**(5), 102-109. http://dx.doi.org/10.15951/j.tmgcxb.2014.05.017

Ye, S.H., Zhao, Z.F., and Zhu, Y.P. (2019). "Large-scale shaking table model test of loess slope supported by frame anchors." *Rock and Soil Mechanics*, **40**(11), 4240-4248. http://dx.doi.org/10.16285/j.rsm.2018.2320

Zhu, Y.P. and Ye, S.H. (2011). "Simplified analysis of slope supported with frame-anchors under lateral seismic loading." *Engineering Mechanics*, **28**(12), 27-32. http://dx.doi.org/10.1097/RLU.0b013e3181f49ac7

Zhuang, J.Q., Peng, J.B., Xu, C., Li, Z.H., Densmore, A., Milledge, D., Iqbal, J., and Cui, Y.F. (2018). "Distribution and characteristics of loess landslides triggered by the 1920 Haiyuan Earthquake, Northwest of China." *Geomorphology*, **314**, 1-12. https://doi.org/10.1016/j.geomorph.2018.04.012.